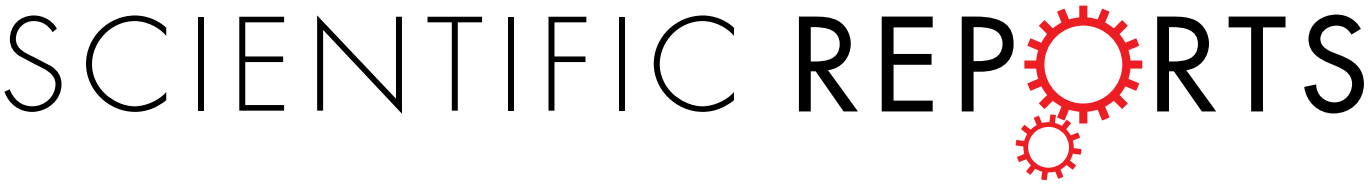

OPEN

Hydrogen-bond potential for ice VIII-X phase transition

Xi Zhang[1], Shun Chen[2] & Jichen Li[2]

Received: 31 May 2016
Accepted: 25 October 2016
Published: 14 November 2016

Repulsive force between the O-H bonding electrons and the O:H nonbonding pair within hydrogen bond (O-H:O) is an often overlooked interaction which dictates the extraordinary recoverability and sensitivity of water and ice. Here, we present a potential model for this hidden force opposing ice compression of ice VIII-X phase transition based on the density functional theory (DFT) and neutron scattering observations. We consider the H-O bond covalent force, the O:H nonbond dispersion force, and the hidden force to approach equilibrium under compression. Due to the charge polarization within the O:H-O bond, the curvatures of the H-O bond and the O:H nonbond potentials show opposite sign before transition, resulting in the asymmetric relaxation of H-O and O:H (O:H contraction and H-O elongation) and the H^+ proton centralization towards phase X. When cross the VIII-X phase boundary, both H-O and O:H contract slightly. The potential model reproduces the VIII-X phase transition as observed in experiment. Development of the potential model may provide a choice for further calculations of water anomalies.

The physical origin and theoretical reproduction of the measured anomalies of water and ice remains a great challenge[1–9]. For example, under compression of the O:H-O bond, the H-O covalent bond becomes longer while the total O–O distance is shortened, leading to the proton centring in the O–O of ice VIII-X phase transition[2,10–14]. The behaviour of the proton is so strange that thermal fluctuation[15] and quantum effect of nuclei[16] were both considered contributing to the ambiguous behaviour. Unlike other materials whose phonons were harden by external pressure, ice-VIII demonstrated the anomalous softening of the H-O vibration mode at frequency greater than 3000 cm^{-1} while stiffening of the O:H vibration mode at frequency lower than 400 cm^{-1} [17–20]. Ice melts under compression and freezes again when the pressure is relieved, evidencing extraordinary recoverability of O:H-O bond[21]. Hydrogen bond interaction potential, typical double-well potentials of the symmetrical[22] and the asymmetrical[23] forms, is still under debate.

An accurate description of the H-bonding between water-water molecules is widely recognised as the crucial factor in the understanding of water anomalies[9,24–26]. Progresses has been made by considering the flexibility of the covalent bonding in water/ice in models such as the flexible-SPC[27] and TIP4PF[28]. Kumagai *et al.* have proposed a flexible KKY potential which has three separate terms: V_{HO}, V_{HH} and V_{OO} in order to account the intra- and inter-molecular interactions separately[11] and adopted by our previous MD calculation[29]. However, since those models have not distinguished O–O linked by O:H-O or not, the reproduction of the proton centring of ice VIII-X has seldom been reported. *Ab initio* MD (AIMD) enabled people to use the *ab initio*-derived force field, though time-expensive. Bernasconi *et al.*[15,30] reproduced the ice VIII/VII/X phase transition by AIMD-derived lattice relaxation and infrared spectra. Sugimura *et al.*[9,11] determined the intermediate structure during the ice VII/X phase transition using AIMD. Katoh *et al.*[31,32] confirmed the fast protonic diffusion coefficient at high temperature molecular phase of ice VII. However, previous researches mostly focused on the structure determination or proton transferring, while the mechanism of the proton centring and the cooperative relaxation of the O:H and H-O are not fully understood. A potential model for time-saving calculations of the proton centring in the ice VIII/X phase transition is still lacking.

Recent progresses find that the hidden force[33], i.e. the repulsive force between the H-O bonding electrons and the O:H nonbonding pair within a O:H-O bond, should play a significant role in various anomalies of water and ice, such as extraordinary recoverability, skin lubricity, etc.[33–36]. For example, in the temperature range from 250 K to 277 K, H-O covalent bond exhibit the normal thermal expansion, while O:H nonbond shrinks due to the reducing repulsive force, leading to the contraction of the total O–O distance[34,36]. At the skin of ice, due to

[1]Institute of Nanosurface Science and Engineering & Guangdong Provincial Key Laboratory of Micro/Nano Optomechatronics Engineering, Shenzhen University, Guangdong, 518060, China. [2]School of Physics and Astronomy, the University of Manchester, Manchester, M13 9PL, UK. Correspondence and requests for materials should be addressed to X.Z. (email: zh0005xi@szu.edu.cn) or J.L. (email: j.c.li@manchester.ac.uk)

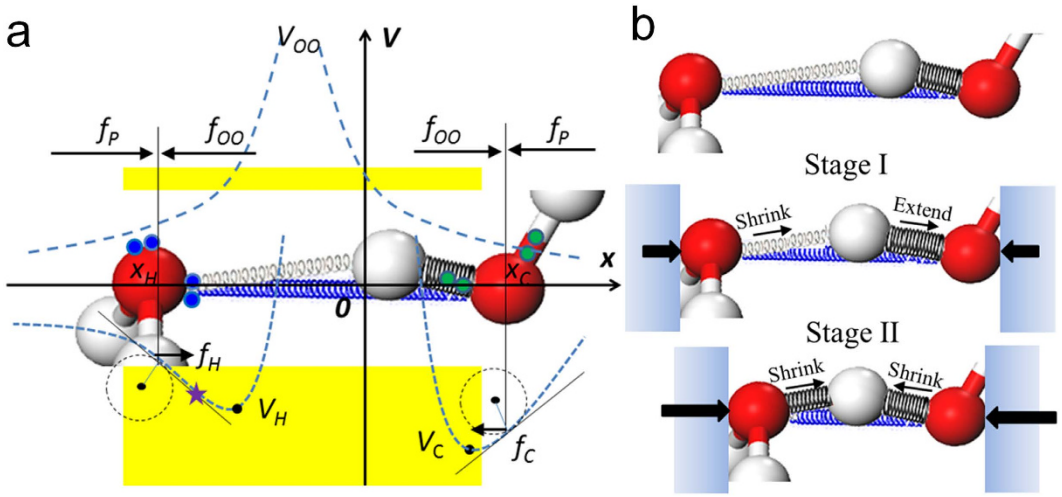

Figure 1. (**a**) Hidden force model for O: H-O bond. x_H and x_C are the O atomic position counting from x = 0 (H atom). f_{OO} is the hidden repulsive force. f_P is the external compression force. f_H and f_C are the recovery force of O:H and O-H, in value of slope of the potential curves (blue dash lines) of V_H and V_C. Star represents the curvature turning point. (**b**) Two stages of O:H-O relaxation under compression. Stage I (ice VIII): A small external force compresses the O:H at first since O:H interaction is weaker than O-H. f_{oo} is then increased to extend O-H. Stage II (ice X): under a large external force, f_H goes across the curvature turning point, leading to the shrinks of both O:H and O-H.

the decrease of the molecular coordination, H-O covalence bond contracts spontaneously to lower the cohesive energy, and hence O:H nonbond is polarized, leading to the surface lubricity[35,37]. This force is beyond the conventional intra- and inter-molecular interactions but depending on the existence of the O:H-O link, i.e. if there is no O:H-O bond like between two O atoms in difference sublattice in ice VIII, hidden force (3 times stronger than Van de Vaals force) interaction would not show[38]. However, it has still seldom reported to address the hidden force of O:H-O bond in a H-bond model, although the force plays a significant role in altering the properties of water and ice.

In this paper, in order to investigate the strange behaviour of proton centring in phase VIII-X transition, we clarified a hidden force model considering the quantum interactions between electron clouds of covalent bond and nonbond and reproduced the anomalous behaviour of proton in ice VIII-X transition.

Potential Model Proposed

Based on our extensive investigation of water anomalies[21,34–36], we proposed hidden force model for dynamics of the "O: H-O" bond under external pressures, as shown in Fig. 1a. In the model, "O: H-O" bond is similar to be connected by three "non-harmonic converted to anharmonic springs". Black spring represents covalent bonding of H-O (denoted as subscript C); Grey spring represents van der Waals interaction between lone pair (blue circles) and proton of O:H (denoted as subscript H); Blue spring represents repulsive interaction between bonding electron pair and lone pair (denoted as subscript OO, but the interaction is not the conventional O–O coulomb repulsion). A water molecule is surrounded by four nearest neighbours (Pauling's ice rule). Four identical O: H-O forms a tetrahedron as the basic unit of water structure (Supplementary Fig. S1). The bond length (x), forces (f) and potential(V) of O:H, H-O and O–O need to reach to a balance under external force (f_p). Figure 1b shows two stages of O:H-O relaxation under compression.

In stage I, a small external force compresses the O:H at first since O:H interaction is weaker than O-H. The repulsive f_{oo} then is increased by the contraction of O…O, leading to H-O extension. In stage II, under a large f_p, f_H goes across the curvature turning point, leading to the shrinks of both O:H and O-H. Intermediate phases exist during the transition where proton disordered symmetrization occurs with delocalized proton in a relatively broad potential well. The delocalization of proton (or proton-transfer) may attributed to quantum effect of nuclei[16,39], or to thermal fluctuations obtained by AIMD[15]. In this work, we focus on the proton centring due to electron interactions within the O:H-O bond.

Without external force, taking centre proton as reference, three springs can reach to equilibrium with their forces along the directions as indicated in Fig. 1a. Due to the f_{oo}, both O atoms are pushed away a little from their lowest-energy positions in the potentials of isolated bonds. Thus, the initial potential recovery forces f_C and f_H will both point inward to center proton; while repulsive force f_{OO} will point outward. Supposing $x_{OO} \cong x_H + x_C$, at equilibrium, total forces (force values) added on O atoms should both be zero:

$$\begin{cases} f_{OO}(x_{C0} + x_{H0}) - f_C(x_{C0}) = 0 \\ f_H(x_{H0}) - f_{OO}(x_{C0} + x_{H0}) = 0 \end{cases} \quad (1)$$

where, x_{C0} and x_{H0} (length values in positive numbers) are the equilibrium position of O atoms counting form $x=0$. Thus, in equilibrium without external force,

$$f_C(x_{C0}) = f_H(x_{H0}) \tag{2}$$

Considering an identical force f_p at both sides, the forces satisfy:

$$\begin{cases} f_{OO}(x_C + x_H) - f_C(x_C) - f_p = 0 \\ f_p + f_H(x_H) - f_{OO}(x_C + x_H) = 0 \end{cases}$$

if

$$\begin{aligned} x_C = x_{C0} + \mathbf{\delta x_C},\ x_H = x_{H0} + \mathbf{\delta x_H} \\ f_C(x_{C0} + \mathbf{\delta x_C}) = f_H(x_{H0} + \mathbf{\delta x_H}) \end{aligned} \tag{3}$$

Supposing the displacement $\mathbf{\delta x}$ is small enough to consider k as a constant, since $k = \frac{\partial f}{\partial x} = -\frac{\partial^2 V}{\partial x^2}$, combining eq. (2) and eq. (3), we can get:

$$k_C \mathbf{\delta x_C} = k_H \mathbf{\delta x_H} \tag{4}$$

Eq. (4) tells us:

i) The values of $\mathbf{\delta x_C}$ and $\mathbf{\delta x_H}$ should be determined by the potential forms of V_H and V_C. Since O:H bond is much longer and weaker than H-O bond, V_H is more flat (smaller curvature) than V_C, i.e. $|k_C| > |k_H|$. Thus, the value of $\mathbf{\delta x_H}$ is always larger than $\mathbf{\delta x_C}$.
ii) If $\mathbf{\delta x_C}$ and $\mathbf{\delta x_H}$ have opposite signs, i.e. x_C and x_H do not both increase or decrease together, k_H and k_C must have opposite sign with each other, which means the curvatures of potentials are opposite, as shown in Fig. 1a.
iii) If $\mathbf{\delta x_C}$ and $\mathbf{\delta x_H}$ have same signs, i.e. x_C and x_H both increase or decrease together, k_H and k_C must have the same sign.

Due to the charge polarization within the O:H-O bond, the curvature of the H-O potential has the opposite sign with O:H potential in the low-pressure region, leading to the contraction of O:H bond but extension of H-O bond and the proton centring. Hence, for O: H-O bond relaxation under external f_p, there are two stages as shown in Fig. 1b:

i) Stage I (ice VIII): in quasi-static process, external force contracts the O:H bond but extends the H-O bond with the total O–O length shortened, when $k_C \cdot k_H < 0$. Both the work of f_P and the change of V_C provide energy for increase of V_H and work of f_{OO}:

$$\begin{aligned} f_P \cdot (\delta x_C + \delta x_H) + \int_0^{\delta x_C} V_C(x_C + \delta x_C)dr = \\ \int_0^{\delta x_{OO}} V_{OO}(x_{OO} + \delta x_C + \delta x_H)dr + \int_0^{\delta x_H} V_H(x_H + \delta x_H)dr \end{aligned} \tag{5}$$

ii) Stage II (ice X): external force is strong enough to make x_H shrink over the curvature turning point (star in Fig. 1) and $k_C \cdot k_H > 0$. External force contract both segments, pushing O atoms back towards the energy-lowest positions, compressing all the three springs. In this case, f_P and energy increases for both segments provides the sharp increase of the V_{OO}:

$$\begin{aligned} f_P \cdot (\delta x_C + \delta x_H) + \int_0^{\delta x_H} V_H(x_H + \delta x_H)dr + \int_0^{\delta x_C} V_C(x_C + \delta x_C)dr = \\ \int_0^{\delta x_{OO}} V_{OO}(x_{OO} + \delta x_C + \delta x_H)dr \end{aligned} \tag{6}$$

Calculations and Verifications. To verify and quantify our potential model, we performed density functional theory (DFT) calculation using CASTEP. The generalized gradient approximation (GGA) function of PW91, HCTH and RPBE were used to describe the exchange–correlation effects (results show little differences among the different functions and hence the PW91 results were presented here). The van der Waals force was also examed by adopting the DFT-D, its effect to the stability of the ice structures has reported, a small effect of red-shifts (~2 meV) for the main peaks of the vibrational spectra was observed. The phonon spectra were calculated using the CASTEP module with finite displacement method. The force constants produced by the CASTEP for the phonon spectra calculations were obtained from the output files. The force for the atom i, f_i ($= \mathrm{d}E/\mathrm{d}r_i$), is simply the derivative of the total energy E. By applying a second small displacement for the atom j, the force constant k_{ij} ($= \mathrm{d}U/\mathrm{d}r_i\mathrm{d}r_j$) is obtained for the pair atoms i and j. A force constant matrix $\mathbf{k}$ for the unit cell is a $3N \times 3N$ matrix (where N is total number of atoms in the unit cell) and were constructed based on above procedure.

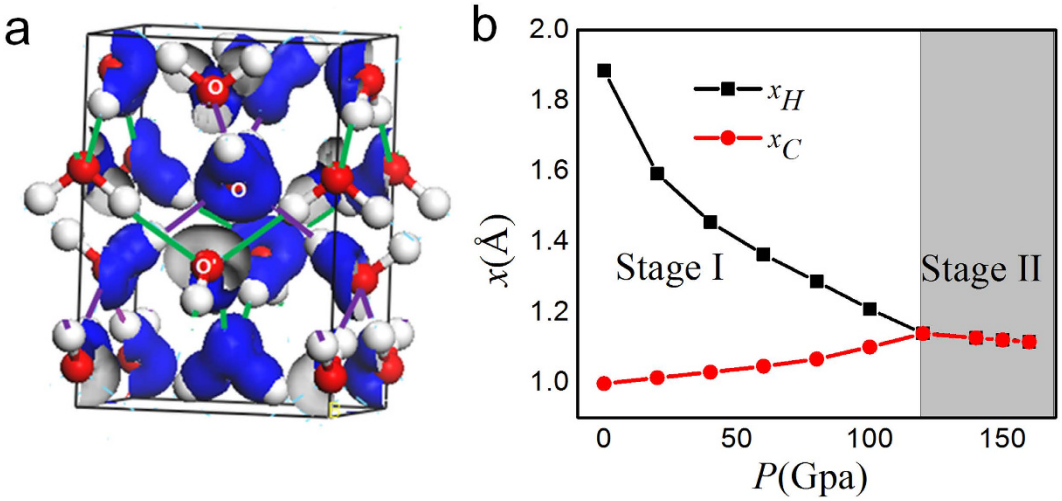

Figure 2. (**a**) Structure of ice VIII. Two nested sublattices connected by green and purple lines respectively are shown. The oxygen atoms in the same sublattice were denoted as O and in the other sublattice as O'. Deformation electron density was plotted as blue isosurface. (**b**) DFT-derived bond length of O:H(x_H) and O-H(x_C) versus pressure. The changing trend of x_H and x_C falls into two stages.

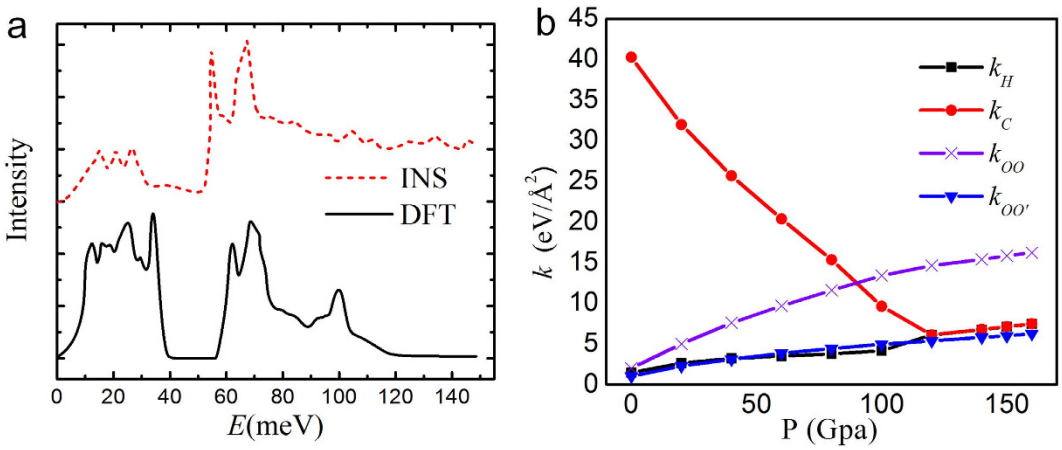

Figure 3. (**a**) Phonon spectra of ice VIII measured using inelastic neutron scattering and calculated uing DFT. (**b**) Force constants of O-H, O:H, O–O in O:H-O bonding and O–O' without bonding.

Ice VIII has a cubic structure containing two sets of interpenetrated ice sub-lattices as shown in Fig. 2a. Hence, each water molecule has 8 nearest neighbours, 4 of them are H-bonded and the others are not, at almost the same O–O distance. The oxygen atoms in the same sublattice were denoted as O and in the other sublattice as O'. Blue isosurface of deformation electron density (density difference before and after bonding,) indicates the position of the bonding electron pair and the O:H nonbond pair. The charge distribution in a water molecule was polarized in the tetrahedral directions by the O:H-O bond. Figure 2b shows the pressure-dependent bond length of O:H(x_H) and O-H(x_C). Proton centring is obtained as pressure increases, in accord with the experimental observation[2,12] and other DFT calculation[33]. The changing trends of x_H and x_C verify the two stages of O:H-O under compression. x_H shrinks and x_C extends in stage I. As pressure increases, x_H and x_C both shrink in stage II like normal material.

The DFT calculation can reproduce phonon spectrum for Ice VIII as shown in Fig. 3a. The simulation reproduces the main features of inelastic neutron scattering (INS) spectrum[24], such as the three peaks in the translational region (<50 meV) and the two sharp peaks of the librational region at about 65 meV. The small peak in the right hand side of librational region at about 100 meV was not shown in the INS spectra due to large Debye-Waller effect in the measured spectra which smeared the spectra dramatically at higher energy transfer. Force constants k_C, k_H and k_{OO} were also obtained from the calculation of phonon spectrum of the ice VIII and are plotted as a function of pressure in Fig. 3b. Apart from the trend for the k_C, k_B to merge at $x_{OO} = 2.3$ Å the force constants between the H-bonded O–O atoms k_{OO} also shows a rapid increase under the external pressure. For the non H-bonded O…O' atoms between the two sub-lattices of ice VIII, a new force constant, $k_{OO'}$ was obtained which remains at small values around k_H. This implies that the O–O interaction only becomes relevant

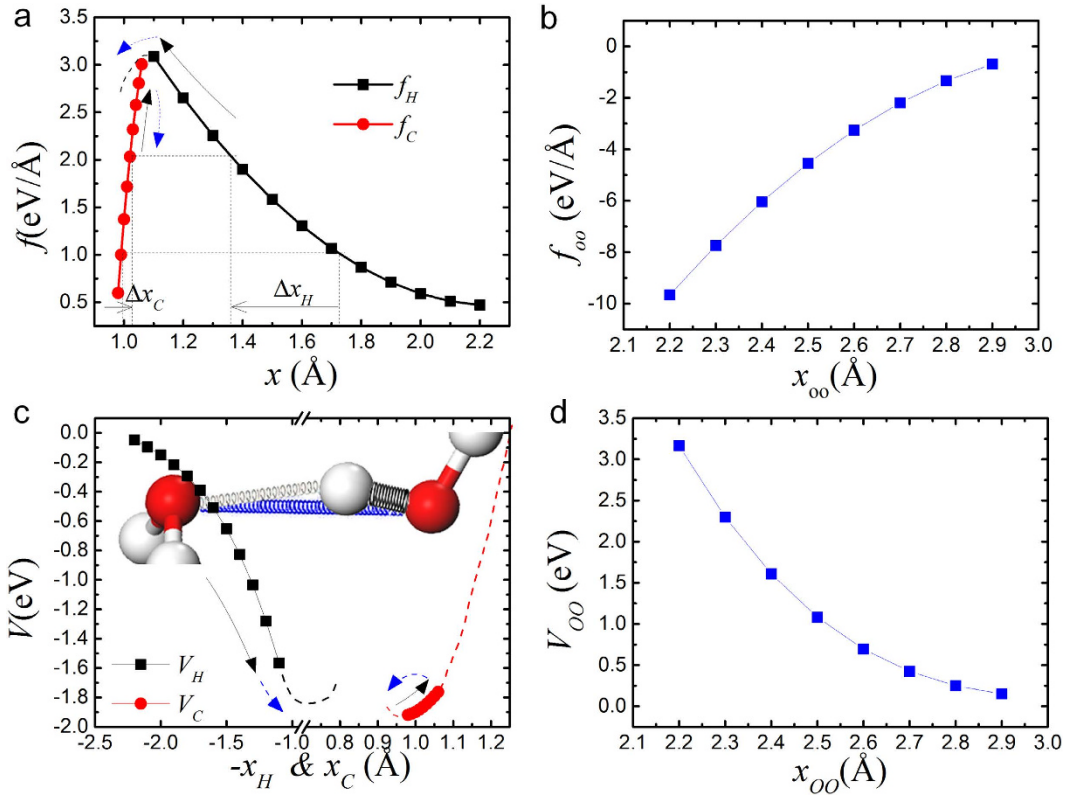

Figure 4. The DFT-fitting curves of bond length x-dependent (**a**), f_C and f_H, (**b**), f_{OO}, (**c**), V_C and V_H, and (**d**), V_{OO} according to water model. Black arrows indicate the opposite relaxation in length of x_C and x_H in stage I; Blue arrows indicate the both decreasing in length of x_C and x_H in stage II.

when the two O atoms are linked by an H atom and hence this large value of k_{OO} is not due to the simple coulomb interaction between O atoms. As shown by the isosurface in Fig. 2a, charge distribution was polarized by O:H-O bonding, i.e. the electron clouds were accumulated in the line of O:H-O, leading to the increase of the repulsive force between bonding pair and nonbonding pair of O–O and the decrease of the interaction between O and O'.

Potential Model Parametrization. Fitting from DFT-derived k-x results of stage I of P-dependent IceVIII (Fig. 3b), we get the relations among k_i and x_i (I = H, C, OO) according to our potential model,

$$\begin{pmatrix} k_H \\ k_C \\ k_{OO} \end{pmatrix} = \begin{pmatrix} a_H & b_H \\ a_C & b_C \\ a_{OO} & b_{oo} \end{pmatrix} \begin{pmatrix} x_H & x_C & x_{OO} \\ 1 & 1 & 1 \end{pmatrix} = \begin{pmatrix} 3.96125 & -8.91589 \\ -289.37672 & 325.26263 \\ -21.26174 & 67.04064 \end{pmatrix} \begin{pmatrix} x_H & x_C & x_{OO} \\ 1 & 1 & 1 \end{pmatrix} \quad (7)$$

where we add negative sign on k_H since DFT only take the positive square root value. Based on k-x curve, we fit the expression of f-x and V-x curves (Supplementary Eq. S1 and S2). The shapes of f-x and V-x are plotted in Fig. 4.

In stage I, as f_p increases, $f_H = f_C$ should also increases according to Eq.(3). Thus, x_H decreases while x_C increases as indicated by black arrows in Fig. 4a. In stage II, when x_H decreases to about 1.1 and reach to the curvature turning point, f_H changes to decrease and x_C will decreases back (as shown by blue arrows) to make $f_C = f_H$. The absolute value of repulsive force f_{OO} always increases as distance x_{OO} decreses. We focus on the parametrization of stage I in this work since it is more interesting than the normal compression-contraction in stage II.

Hence, for a given f_P, there is only one set of solutions of x_H and x_C obtained in Fig. 5. Figure 5a shows that, for a given x_H, $f_H = f_C$ gets the x_C. Then, Fig. 5b shows that, f_{OO} can be calculated by $x_H + x_C$ and f_P is correlated with x_H by $f_p = f_{OO} - f_H$. Hence, we have obtained the f_P-x_H curve in Fig. 5b, from which a given external f_P can determine the relaxation of x_H and x_C. Thus, the correlations among external compression force, the length relaxation of H-O and O:H bond, the forces of O-H, O:H and O:O are all determined. Figure 5b also indicates that, as f_P increases, f_{OO} rises much more significantly than f_H. Thus, f_{OO} is indeed a hidden force that should not be ignored.

Based on our potential model, foo, f_H and fp are functions of x_H and x_C determined by Supplementary Eq. S1 and Fig. 4. We run the time-dependent dynamic process of external pressure on O:H-O bond in Fig. 6. The dynamic equation can be expressed as:

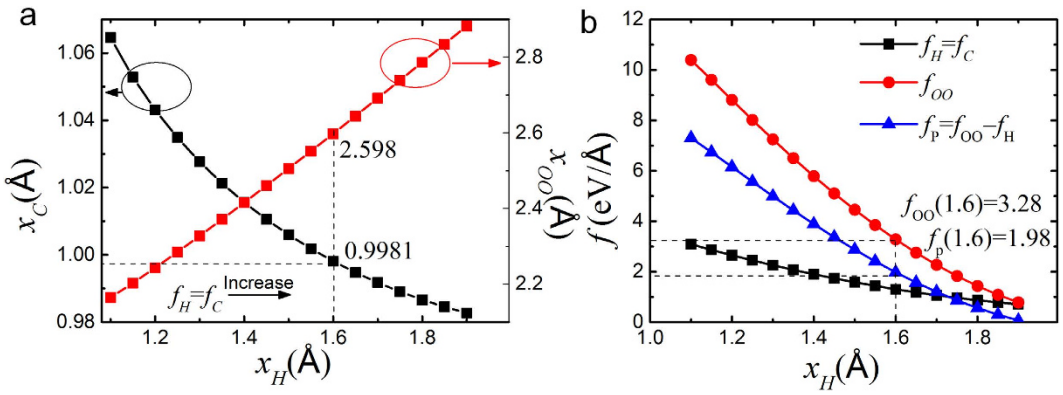

Figure 5. (**a**) Correlation between x_H and x_C. (**b**) Correlation of x_H, f_P. f_H, and f_{OO}. Under external f_p, the length and force relaxations inside the O:H-O bonding are all determined.

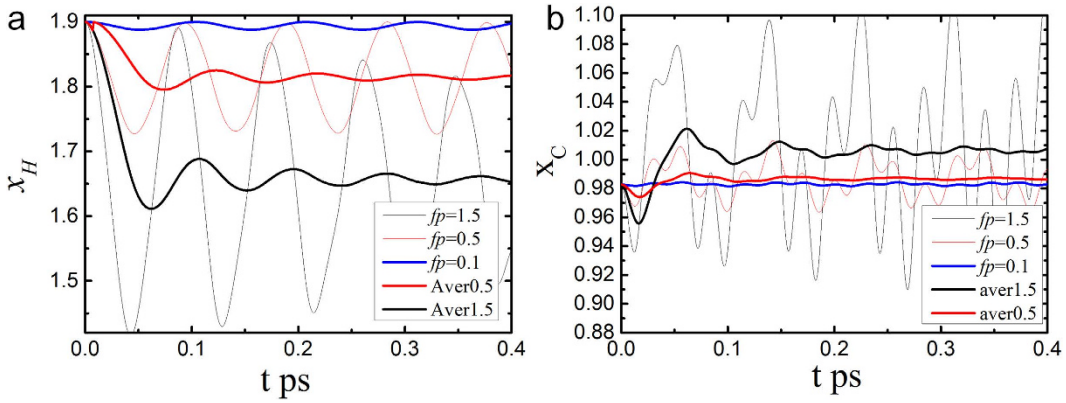

Figure 6. Time-dependent relaxation dynamics of O:H-O bond with the same initial lengths and different external forces. (**a**) x_H relaxes with time and (**b**), x_C relaxes with time under $fp = 0.1$, 0.5 and 1.5 eV/Å. The initial lengths are 1.9 and 0.98269 at 0 external force, which give initial energies for bonds to oscillate around the equbrillium point under pressures. x_H and x_C under $fp = 0.5$ and 1.5 eV/Å were taken average.

$$\begin{cases} \mu\dfrac{d^2x_H}{dt^2} = |f_{OO}| - |f_H| - |f_P| \\ \mu\dfrac{d^2x_C}{dt^2} = |f_{OO}| - |f_C| - |f_P| \\ x_H = 1.9,\ x_C = 0.98269 \qquad (t = 0) \\ v_H = v_C = 0 \qquad (t = 0) \end{cases} \tag{8}$$

The initial condition of x_H and x_C are the lengths (Å) without pressure. The partial differential equation is solved by 4th order Runge-Kutta method (Supplementary Method).

Figure 6 shows the x_H and x_C relaxation with the same initial lenghs and different external forces under $f_p = 0.1$, 0.5 and 1.5 eV/Å. The initial lengths are bond lengths at fp = 0, which give energies to atoms to oscillate. If the process is slow, i.e. initial coordinates are around the stable point, the oscillation will decrease. x_H and x_C under $fp = 0.5$ and 1.5 eV/Å were taken average as $(\sum_0^t x_{C/H}(t))/t$. The results show that, as fp increases, x_H decreases from 1.890 to 1.811 and to 1.645 Å in average, while x_C increases from 0.983 to 0.992 and to 1.015 Å in average, agreeing well with proton centring obtained both in DFT calculation and experimental observation[2,12].

Figure 7 a and b show the time-dependent dynamics of O:H-O bond in the quasi-static process under fp from 0.1 to 0.5 eV/Å. The initial lengths at each fp were taken as the average bond lengths of the previous fp. Hence, bond length relaxes more stably with time. Figure 7c shows the average bond lengths obtained from the quasi-static states at different fp. The dynamic curves oscillated stably raise the reliability of the average lengths. Results show that as fp increases, O:H bond length decreases and H-O bond length increases, approaching to equal at about $fp = 6.91$ eV/Å. the Therefore, upon compression, in the equilibrium status of O:H-O, proton and oxygen shift both towards the other oxygen while proton shift a little to the weaker O:H part. Besides, O:H vibrates much slower than H-O bond due to its weaker force constant, as indicated by the frequency of the relaxation curves.

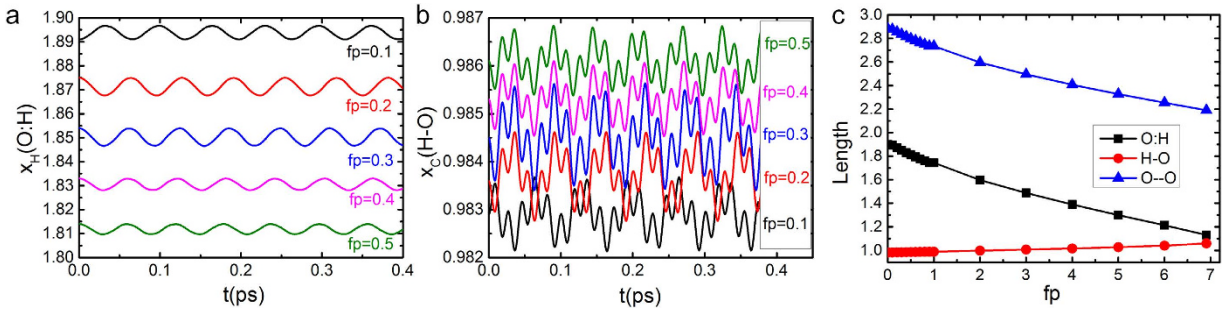

Figure 7. Time-dependent dynamics of O:H-O bond in the quasi-static process, with different initial bond lengths. (**a**) x_H relaxes with time and (**b**), x_C relaxes with time under *fp* from 0.1 to 0.5 eV/Å. The initial lengths at each *fp* were taken as the average bond lengths of the previous *fp*. Hence, the oscillations of bonds were largely reduced. (**c**), the average bond lengths derived at *fp* from 0.1 to 6.91 eV/Å. Proton centring occurs near $fp = 6.91$ eV/Å.

The potential model of O:H-O can be further applied to water molecules and crystal structures considering the interactions of H—H and O–O'. $V_{OO'}$ follows the weak dispersion interaction as indicated by the force constant developed by DFT in Fig. 3b, since electron cloud distributes mostly on the line of O:H-O bond as shown in Fig. 2a. Current potential model provides an efficient tool to investigate bond length relaxation, time-dependent proton dynamics, mass density and intermediate structure determination of dense ice phases.

Conclusion

DFT and neutron scattering observations have enabled a O:H-O bond potential for the ice VIII-X phase transition under compression. Before transition, H-O undergoes elongation and the O:H compression because of the O:H-O bond segmental disparity and O-O repulsion; after transition, both H-O and O:H undergoes slight contraction because of the excessive compression. The effectiveness of current potential model was illustrated when dealing with H-bonded systems under pressure. More importantly, this additional force could provide the necessary mechanism to explain a range of water anomalies, for instance the complex phase diagram, i.e. its morphism, this is probably because the hydrogen bonds become very easy to buckle under the extra strong O–O interaction if the O:H-O is not in straight line. This hidden force, f_{OO} has often been overlooked experimentally in the past, perhaps because it is easily concealed by the f_H and f_C. The hidden force potential model reproduced the contraction of O:H bond and extension of H-O bond and the proton centralization under compression. The potential model to develop further can serve as a key for theoretical reproduction of the O:H-O bond asymmetric relaxation under external stimuli.

References

1. Goncharov, A. F., Struzhkin, V. V., Mao, H.-k. & Hemley, R. J. Raman Spectroscopy of Dense H2O and the Transition to Symmetric Hydrogen Bonds. *Phys. Rev. Lett.* **83,** 1998 (1999).
2. Benoit, M., Marx, D. & Parrinello, M. Tunnelling and zero-point motion in high-pressure ice. *Nature* **392,** 258–261 (1998).
3. Frenken, J. W. M. & Oosterkamp, T. H. MICROSCOPY When mica and water meet. *Nature* **464,** 38–39, doi: 10.1038/464038a (2010).
4. Headrick, J. M. *et al.* Spectral signatures of hydrated proton vibrations in water clusters. *Science* **308,** 1765–1769, doi: 10.1126/science.1113094 (2005).
5. Gregory, J. K., Clary, D. C., Liu, K., Brown, M. G. & Saykally, R. J. The Water Dipole Moment in Water Clusters. *Science* **275,** 814–817, doi: 10.1126/science.275.5301.814 (1997).
6. Bjerrum, N. Structure and properties of ice. *Science* **115,** 385–390 (1952).
7. Soper, A. K., Teixeira, J. & Head-Gordon, T. Is ambient water inhomogeneous on the nanometer-length scale? *Proc. Natl. Acad. Sci. USA.* **107,** E44–E44, doi: 10.1073/pnas.0912158107 (2010).
8. Zha, C.-S., Hemley, R. J., Gramsch, S. A., Mao, H.-k. & Bassett, W. A. Optical study of H2O ice to 120GPa: Dielectric function, molecular polarizability, and equation of state *J. Chem. Phys.* **126,** 074506, doi: 10.1063/1.2463773 (2007).
9. Iitaka, T., Fukui, H., Li, Z., Hiraoka, N. & Irifune, T. Pressure-induced dissociation of water molecules in ice VII. *Sci Rep* **5,** 12551, doi: 10.1038/srep12551 (2015).
10. Loubeyre, P., LeToullec, R., Wolanin, E., Hanfland, M. & Husermann, D. Modulated phases and proton centring in ice observed by X-ray diffraction up to 170 GPa. *Nature* **397,** 503–506 (1999).
11. Sugimura, E. *et al.* Compression of H2O ice to 126 GPa and implications for hydrogen-bond symmetrization: Synchrotron x-ray diffraction measurements and density-functional calculations. *Physical Review B* **77,** 214103 (2008).
12. Kang, D., Dai, J., Hou, Y. & Yuan, J. Structure and vibrational spectra of small water clusters from first principles simulations. *J. Chem. Phys.* **133,** 014302 (2010).
13. Holzapfel, W. B. On the Symmetry of the Hydrogen Bonds in Ice VII. *The Journal of Chemical Physics* **56,** 712–715 (1972).
14. Bhatt, H. *et al.* Hydrogen Bond Symmetrization in Glycinium Oxalate under Pressure. *The Journal of Physical Chemistry B* **120,** 851–859, 10.1021/acs.jpcb.5b11507 (2016).
15. Bernasconi, M., Silvestrelli, P. L. & Parrinello, M. Ab Initio Infrared Absorption Study of the Hydrogen-Bond Symmetrization in Ice. *Phys. Rev. Lett.* **81,** 1235–1238 (1998).
16. Meng, X. *et al.* Direct visualization of concerted proton tunnelling in a water nanocluster. *Nat Phys* **11,** 235–239, doi: 10.1038/nphys3225 (2015).
17. Yoshimura, Y., Stewart, S. T., Somayazulu, M., Mao, H. & Hemley, R. J. High-pressure x-ray diffraction and Raman spectroscopy of ice VIII. *J. Chem. Phys.* **124,** 024502, doi: 10.1063/1.2140277 (2006).
18. Pruzan, P. *et al.* Phase diagram of ice in the VII–VIII–X domain. Vibrational and structural data for stronglycompressed ice VIII. *J. Raman Spectrosc.* **34,** 591–610 (2003).

19. Song, M., Yamawaki, H., Fujihisa, H., Sakashita, M. & Aoki, K. Infrared absorption study of Fermi resonance and hydrogen-bond symmetrization of ice up to 141 GPa. *Physical Review B* **60,** 12644 (1999).
20. Santra, B. *et al.* Hydrogen Bonds and van der Waals Forces in Ice at Ambient and High Pressures. *Phys. Rev. Lett.* **107,** 185701 (2011).
21. Zhang, X. *et al.* Ice Regelation: Hydrogen-bond extraordinary recoverability and water quasisolid-phase-boundary dispersivity. *Scientific Reports* **5,** 13655, doi: 10.1038/srep13655 (2015).
22. Teixeira, J. High-pressure physics - The double identity of ice X. *Nature* **392,** 232–233 (1998).
23. Kumagai, T. Direct observation and control of hydrogen-bond dynamics using low-temperature scanning tunneling microscopy. *Prog. Surf. Sci.* **90,** 239–291, doi: 10.1016/j.progsurf.2015.04.001 (2015).
24. Li, J. & Ross, D. K. Evidence for two kinds of hydrogen bond in ice. *Nature* **365,** 327–329 (1993).
25. Zhang, L.-J., Wang, J., Luo, Y., Fang, H.-P. & Hu, J. A novel water layer structure inside nanobubbles at room temperature *Nuclear Science and Techniques* **25,** 060503, doi: 10.13538/j.1001-8042/nst.25.060503 (2014).
26. Gaffney, K. J., Ji, M., Odelius, M., Park, S. & Sun, Z. H-bond switching and ligand exchange dynamics in aqueous ionic solution. *Chem. Phys. Lett.* **504,** 1–6, doi: 10.1016/j.cplett.2011.01.063 (2011).
27. Toukan, K. & Rahman, A. Molecular-dynamics study of atomic motions in water. *Physical Review B* **31,** 2643–2648 (1985).
28. Lawrence, C. P. & Skinner, J. L. Flexible TIP4P model for molecular dynamics simulation of liquid water. *Chem. Phys. Lett.* **372,** 842–847, doi: 10.1016/S0009-2614(03)00526-8 (2003).
29. Burnham, C. J., Li, J. C. & Leslie, M. Molecular Dynamics Calculations for Ice Ih. *The Journal of Physical Chemistry B* **101,** 6192–6195, doi: 10.1021/jp9632596 (1997).
30. Benoit, M., Romero, A. H. & Marx, D. Reassigning Hydrogen-Bond Centering in Dense Ice. *Phys. Rev. Lett.* **89,** 145501 (2002).
31. Cavazzoni, C. *et al.* Superionic and Metallic States of Water and Ammonia at Giant Planet Conditions. *Science* **283,** 44–46, doi: 10.1126/science.283.5398.44 (1999).
32. Eriko Katoh, H. Y., H. Fujihisa, M. Sakashita & K. Aoki. Protonic Diffusion in High-Pressure Ice VII. *Science* **295,** 1264–1266, doi: 10.1126/science.1067746 (2002).
33. Sun, C. Q., Zhang, X. & Zheng, W. The hidden force opposing ice compression. *Chemical Science* **3,** 1455–1460 (2012).
34. Huang, Y. *et al.* Hydrogen-bond relaxation dynamics: Resolving mysteries of water ice. *Coord. Chem. Rev.* **285,** 109–165, doi: 10.1016/j.ccr.2014.10.003 (2015).
35. Zhang, X. *et al.* Water Nanodroplet Thermodynamics: Quasi-Solid Phase-Boundary Dispersivity. *The Journal of Physical Chemistry B* **119,** 5265–5269, 10.1021/acs.jpcb.5b00773 (2015).
36. Zhang, X. *et al.* Water's phase diagram: From the notion of thermodynamics to hydrogen-bond cooperativity. *Prog. Solid State Chem.* **43,** 71–81, doi: 10.1016/j.progsolidstchem.2015.03.001 (2015).
37. Zhang, X., Huang, Y., Ma, Z., Niu, L. & Sun, C. Q. From ice superlubricity to quantum friction: Electronic repulsivity and phononic elasticity. *Friction* **3,** 294–319, 10.1007/s40544-015-0097-z (2015).
38. Shun, C., Zhiping, X. & Jichen, L. The observation of oxygen—oxygen interactions in ice. *New Journal of Physics* **18,** 023052, (2016).
39. Herrero, C. P. & Ramírez, R. Path-integral simulation of ice VII: Pressure and temperature effects. *Chem. Phys.* **461,** 125–136, doi: 10.1016/j.chemphys.2015.09.011 (2015).

Acknowledgements

We would like to thank ISIS of Rutherford-Appleton Laboratory for the access of neutron scattering facilities. The authors thank the support of the National Nature Science Foundation of China (No. 51605306), NSF of Guangdong (No. 2016A030310060), Guangdong Innovation Youth Fund (No. 2015KQNCX144), NSF of SZU (No. 201528, No. 827000131), and Shenzhen foundation fund (No. JCYJ20160427105015701).

Author Contributions

X.Z. proposed the theoretical model. X.Z. and S.C. performed the calculation. S.C. and J.C.L. did the inelastic neutron scattering measurements. X.Z. and J.C.L wrote the main manuscript text. All authors reviewed the manuscript.

Additional Information

Supplementary information accompanies this paper at http://www.nature.com/srep

Competing financial interests: The authors declare no competing financial interests.

How to cite this article: Zhang, X. *et al.* Hydrogen-bond potential for ice VIII-X phase transition. *Sci. Rep.* **6**, 37161; doi: 10.1038/srep37161 (2016).

Publisher's note: Springer Nature remains neutral with regard to jurisdictional claims in published maps and institutional affiliations.